https://doi.org/10.2352/EI.2024.36.15.COIMG-144
© 2024, Society for Imaging Science and Technology

Gradient-Based Image Visualization for Noisy LWIR Image

Taichi Nakano, Masayuki Tanaka, and Masatoshi Okutomi; Tokyo Institute of Technology, Japan

Abstract

The dynamic range of the intensity of long-wave infrared (LWIR) cameras are often more than 8bit and its images have to be visualized using histogram equalization and so on. Many visualization methods do not consider effects of noise, which must be taken care of in real situations. We propose a novel LWIR images visualization method based on gradient-domain processing or gradient mapping. Processing based on intensity and gradient power in the gradient domain enables visualizing LWIR images with noise reduction. We evaluate the proposed method quantitatively and qualitatively and show its effectiveness.

Introduction

A long-wave infrared (LWIR) camera is a device that measures the LWIR radiation emitted from an object and obtains the information as an image. The LWIR radiation emitted from an object is depending on the temperature of the object and is not affected by visible light as is the case with visible cameras. Therefore, an LWIR camera can capture images of objects at night, in dense fog, or in other situations where visible light information is scarce. Taking advantage of this characteristic, researches have been conducted on robust pedestrian detection using LWIR images [13][14][15][16][17], inspection of building structures using LWIR images [18][19][20][21], and image composition of visible and LWIR images [2][9][10][11][12].

Although the dynamic range of intensity of an LWIR camera is very wide, pixel values are often concentrated in the intensity range, which requires visualization processing. Figures 1 (a) and 1 (b) show the results of visualization using percentile normalization (PN) and histogram equalization (HE) [6], respectively. In the percentile normalization (PN), a linear transformation is performed so that the pixel values of the 2.5-th percentile of the image are set to 0 and those of the 97.5-th percentile to 1, taking outliers into account. These processes can spread out the pixel values that were concentrated locally, which increases the contrast and enables the subject to be seen well. On the other hand, the problem of stripe noise or random noise appears.

Contrast-limited histogram equalization (CLHE) [7][8] has been proposed as a method to reduce noise by reducing the contrast of an image (Figure 1 (c)). In contrast-limited histogram equalization (CLHE), the pixel values with high frequencies in the histogram of an image are distributed over the entire range, and then the histogram is equalized. This avoids over-amplification of contrast and allows visualization with less noise. However, it cannot be said that the noise in the image is completely eliminated, and due to the characteristic of the process, the contrast of the output image resulting from the method is in principle lower than that from histogram equalization (HE).

We propose a method to visualize LWIR images while reducing noise by processing in the gradient domain of the image. The gradient features obtained by the differential filter are multiplied by a gain based on pixel values, and then multiplied by another gain calculated from the gradient power. This enables noise components to be reduced in the gradient domain. The gradient is reconstructed using an image reconstruction method that takes into account the range of the image to visualize LWIR images [1].

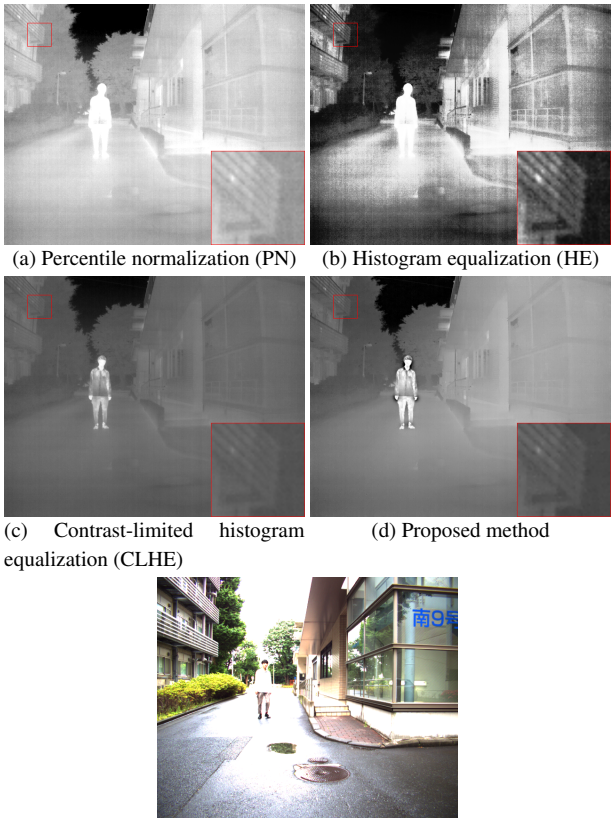

(a) Percentile normalization (PN) (b) Histogram equalization (HE)

(c) Contrast-limited histogram equalization (CLHE) (d) Proposed method

(e) Visible image

Figure 1: Example of LWIR image visualization (Image A)

We experimentally demonstrate that the proposed algorithm can effectively visualize noisy LWIR images. From visual comparisons, the proposed gradient-domain visualization shows better results than existing algorithms. Quantitative comparisons also show effectiveness of the proposed algorithm.

Proposed Method

Overview

Figure 2 shows the overview of the proposed method. The gradient is adjusted in the gradient domain to emphasize important edges while reducing noise components. The details are explained in the next subsection.

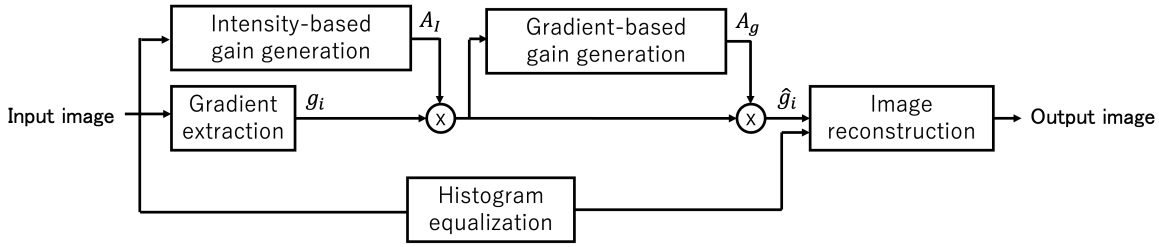

Figure 2: Overview of the proposed method

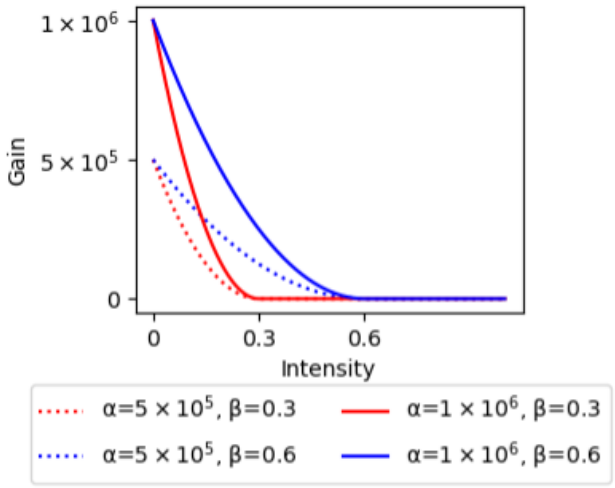

Figure 3: A specific example of the intensity-based gain

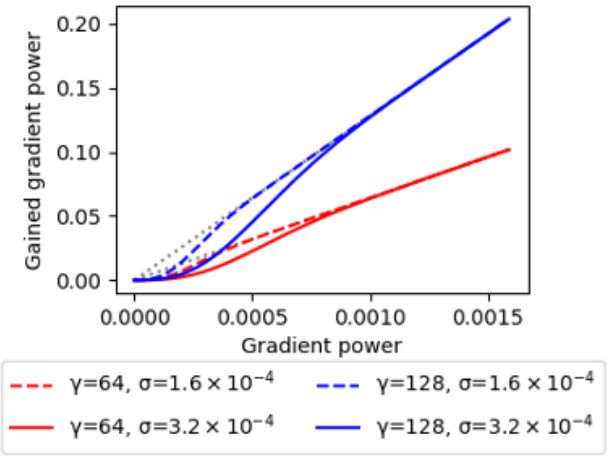

Figure 4: A specific example of the gradient-based gain

Gradient Extraction

The gradient features are extracted from LWIR images by convolving horizontal and vertical forward and backward differential filters. We apply four types of differential filters as gradient features: horizontal forward, horizontal backward, vertical forward, and vertical backward. We denote those gradient features as g_{hf}, g_{hb}, g_{vf} and g_{vb}, respectively.

Gain Adjustment Based on Intensity Value

It is known that the contrast is lower in regions with small intensity values than that in regions with large intensity values, especially in images with a wide dynamic range, such as LWIR images. Therefore, in this study, the gradient corresponding to pixels with small intensity values is amplified to improve the contrast. Specifically, the gain shown in Equation 1 is obtained, and the gradient is multiplied by the gain.

$$A_I[i,j] = \begin{cases} \dfrac{\alpha-1}{\beta^2}(I[i,j]-\beta)^2+1 & (I[i,j]<\beta) \\ 1 & (I[i,j]\geq\beta) \end{cases}, \tag{1}$$

where I is the input image, A_I is the gain based on the intensity value, $[i,j]$ is the pixel position, and α and β are parameters, respectively. As shown in Figure 3, a gain greater than 1 determined by α and β is multiplied to the gradient of a pixel whose intensity value is less than β. Therefore, the gradient is amplified in regions with small intensity values.

Gain Adjustment Based on Gradient Value

In the gradient domain, small gradients are considered as noise. Therefore, we consider attenuating small gradients while amplifying relatively large gradients. For this purpose, we introduce the gain shown in Equation 2.

$$A_g[i,j] = \gamma\left(1-\exp\left(-\frac{g_p^2[i,j]}{2\sigma^2}\right)\right), \tag{2}$$

where $g_p^2[i,j]$ is the gradient power at pixel $[i,j]$ and calculated by

$$g_p^2[i,j] = \frac{1}{2}\sum_{k=h,v}\sum_{l=f,b} g_{kl}^2[i,j]. \tag{3}$$

Here, g_{kl} denotes the horizontal or vertical, forward or backward difference, respectively. γ and σ are parameters. By applying this gain to the gradient feature, the gradient value can be further attenuated for pixels with small gradient values, as shown in Fig. 4.

Image Reconstruction

Based on the method in [1], image reconstruction is performed from gradient features. Specifically, we optimize the objective function $E(\boldsymbol{u})$ in Equation 4.

$$E(\boldsymbol{u}) = F(\boldsymbol{u}) + R(\boldsymbol{u}), \tag{4}$$

where, $\boldsymbol{u}$ is the reconstructed image, $F(\boldsymbol{u})$ denotes the gradient fidelity term, and $R(\boldsymbol{u})$ is the intensity range constraint term.

The gradient fidelity term $F(\boldsymbol{u})$ is expressed by Equation 5.

$$F(\boldsymbol{u}) = \sum_{i,j}\sum_{d=h,v} |u_d[i,j]-q_d[i,j]|^2, \tag{5}$$

where $q_d[i,j]$ represents the target gradient calculated from the gradient features as follows.

$$q_h[i,j] = \frac{\hat{g}_{hf}[i+1,j] + \hat{g}_{hb}[i,j]}{2}, \tag{6}$$

$$q_v[i,j] = \frac{\hat{g}_{vf}[i+1,j] + \hat{g}_{vb}[i,j]}{2}, \tag{7}$$

$$\hat{g}_{kl}[i,j] = A_I[i,j] \cdot A_g[i,j] \cdot g_{kl}[i,j], (k = \{h,v\}, l = \{f,b\}). \tag{8}$$

This gradient fidelity term minimizes the residual between the gradient of the reconstructed image and the target gradient.

The intensity range constraint term $R(\boldsymbol{u})$ is expressed by the following equation.

$$R(\boldsymbol{u}) = \sum_{i,j} r(u[i,j]), \tag{9}$$

$$r(\xi) = \begin{cases} 0 & (R_{min} \leq \xi \leq R_{max}) \\ \infty & (else) \end{cases}, \tag{10}$$

where R_{min} and R_{max} denote the lower and upper limits of the intensity of the reconstructed image, respectively.

The actual optimization process is performed by the proximal gradient method. The update formula for the proximal gradient method is shown in Equation 11.

$$\boldsymbol{u} \leftarrow \mathrm{prox}\left(\boldsymbol{u} - \eta\left(\sum_{d=h,v} \frac{\partial}{\partial d}(\boldsymbol{u}_d - \boldsymbol{q}_d)\right)\right), \tag{11}$$

where $\mathrm{prox}(\cdot)$ denotes the proximal mapping of the intensity range constraint term. The proximal mapping corresponding to Equation 10 is the same as clipping pixel values in the range from minimum R_{min} to maximum R_{max}. As the initial image for the optimization process, the histogram-equalized LWIR image is used.

Experiments

Experimental Details

We compare the results of visualization by percentile normalization (PN), histogram equalization (HE), contrast-limited histogram equalization (CLHE), and the proposed method. The parameters of the proposed method are $\alpha = 1.6 \times 10^4$, $\beta = 0.35$, $\gamma = 128$ and $\sigma = 1.6 \times 10^{-4}$. The limit is set to 1×10^{-5} as the parameter for contrast-limited histogram equalization (CLHE). This value represents the ratio of the number of pixels to the total number of pixels. A FLIR ADK camera was used to capture the LWIR images.

Validation

In order to demonstrate the effectiveness of the two gains in the gradient domain in the proposed method, the following comparisons are conducted.

(1) The case where $\sigma = 0$ in Equation 2 (without noise reduction)
(2) The case where only the gradient-based gain is used (without intensity-based gain)

(a) Without noise reduction (b) Without intensity-based gain

(c) Proposed method

Figure 5: Qualitative comparison of validation

Figure 5 shows the qualitative evaluation of image B. From these results, it can be seen that (a) without noise reduction, noise appears in the entire image. Since only a constant is applied to the gradient, it can be confirmed that noise appears at the same time as the contrast increases. (b) Without intensity-based gain, the noise is reduced, but the contrast is not sufficient in the low intensity region. (c) The proposed method reduces the noise compared to (a), and also improves the contrast in the area of small intensity values compared to (b).

Comparative Experiments

Visualization is performed on eight LWIR images and a quantitative evaluation of these images is performed. A qualitative evaluation of three of them is also performed.

Quantitative Evaluation

Quantitative evaluation of the visualization results from each method is conducted from the following three perspectives: (1) how noisy the image is, (2) how easy it is to see the image in terms of contrast and (3) how much is the signal-to-noise ratio of the image. In addition, as a traditional NRIQA, an evaluation by BRISQUE [4] is also conducted. (4)

(1) In this study, as there are no ground-truth images corresponding to the noisy images, a non-reference image quality assessment (NRIQA) method is required in order to evaluate how noisy the images are. We use the method proposed in [3] as NRIQA. This method utilize an eigenvalue decomposition of the matrix representing the features computed from the image to evaluate how noisy the image is.

(2) We quantitatively evaluate the legibility of the images due to contrast. Based on the assumption that the contrast of an image is high and the image is easily recognized when its pixel values are widely distributed, the standard deviation of all pixel values is used to evaluate this item. The higher this value is, the easier the image is for people to see.

(3) There is thought to be a correlation between image contrast and noise level. Therefore, it is not valid to ignore the contrast of the image and compare only the noise level. For this rea-

Metrics	Method	Image A	Image B	Image C	Image D	Image E	Image F	Image G	Image H	Average
(1) Noise level $n[\times 10^{-2}]$	PN	1.342	1.284	2.851	1.106	1.555	1.749	2.734	2.033	1.832
	HE	3.826	2.517	3.286	2.749	3.643	3.379	3.567	3.145	3.264
	CLHE	**0.571**	**0.595**	**0.630**	**0.591**	**0.699**	**0.553**	**0.616**	**0.512**	**0.596**
	Proposed	0.708	0.764	0.861	0.754	0.735	0.654	0.655	0.702	0.729
(2) Std of intensity s	PN	0.1800	0.2729	0.2615	0.2083	0.1847	0.1925	0.2365	0.2160	0.2191
	HE	**0.2893**	**0.2894**	**0.2889**	**0.2894**	**0.2893**	**0.2890**	**0.2888**	**0.2889**	**0.2891**
	CLHE	0.0849	0.1253	0.0731	0.1162	0.0904	0.0802	0.0682	0.0710	0.0887
	Proposed	0.1566	0.2202	0.1974	0.2056	0.1665	0.2047	0.1599	0.1587	0.1837
(3) Std to noise ratio s/n	PN	13.41	21.25	9.17	18.83	11.88	11.01	8.65	10.62	13.10
	HE	7.56	11.50	8.79	10.53	7.94	8.55	8.10	9.19	9.02
	CLHE	14.85	21.07	11.60	19.67	12.94	14.50	11.08	13.85	14.94
	Proposed	**22.11**	**28.81**	**22.92**	**27.26**	**22.63**	**31.31**	**24.41**	**22.61**	**25.26**
(4) BRISQUE	PN	27.12	27.99	40.35	25.16	30.19	32.37	37.65	34.31	31.89
	HE	31.97	27.44	38.97	**23.03**	33.97	28.93	33.33	32.40	31.26
	CLHE	27.31	**20.93**	31.81	26.10	30.03	30.22	28.46	33.85	28.59
	Proposed	**26.15**	31.21	**27.97**	25.71	**27.23**	**28.86**	**25.69**	**27.96**	**27.60**

Table 1: Quantitative evaluation of visualization results by each method (Bolded text indicates the best results)

son, the value in (2) is divided by the value in (1) to obtain a value corresponding to the signal-to-noise ratio, and the image is evaluated with the value.

Table 1 shows the results of evaluating the visualized images of each method according to the above four items.

(1) For noise level, all the visualization results of CLHE are the best. The visualization results of the proposed method are better than those of PN and HE, which indicates that the noise is successfully reduced in the gradient region.

(a) Percentile normalization (PN)

(b) Histogram equalization (HE)

(c) Contrast-limited histogram equalization (CLHE)

(d) Proposed method

(e) Visible image

Figure 6: Visualization example of Image B

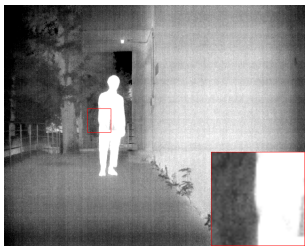

(a) Percentile normalization (PN)

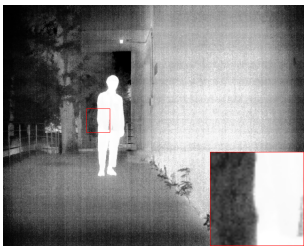

(b) Histogram equalization (HE)

(c) Contrast-limited histogram equalization (CLHE)

(d) Proposed method

(e) Visible image

Figure 7: Visualization example of Image C

(2) For the standard deviation of pixel values, all the visualization results of HE are the largest and have the highest contrast. It can be seen that the visualization results of the proposed method have better results than CLHE.

(3) The ratio of (1) and (2) shows that all the visualization result of the proposed method is the best. This indicates that the proposed method is able to reduce noise in the gradient region while maintaining the contrast of the image.

(4) In BRISQUE, the visualization results of the proposed

method are the best in six out of the eight scenes. In light of the qualitative evaluation that follows, it cannot be said that BRISQUE is an index that necessarily matches human senses in this experiment, but the results may provide evidence to support the effectiveness of the proposed method.

Qualitative Evaluation

Figures 1, 6 and 7 show the results of visualization of images A, B and C, respectively. Images of the same scene taken with a visible camera are also shown for reference. As seen in the overall results, the percentile normalization (PN) and histogram equalization (HE) show a large amount of random noise and stripe noise. In addition, the details of the human parts are not visible due to white-out. Although contrast-limited histogram equalization (CLHE) significantly reduces the noise and takes out white-out of images, it can be seen that the contrast is also reduced. On the other hand, the proposed method succeeds in reducing noise without reducing contrast. In addition, there is no white-out in the human parts, and details can be confirmed.

Conclusion

In this paper, we propose a gain adjustment method in the gradient domain of the image to visualize LWIR images while suppressing noise. Experimental results show that the proposed method produces images with less noise and higher contrast than the methods such as percentile normalization, histogram equalization and contrast-limited histogram equalization. The effectiveness of the two proposed gains is also demonstrated by validation experiments.

References

[1] T. Shibata, M. Tanaka and M. Okutomi, Gradient-Domain Image Reconstruction Framework With Intensity-Range and Base-Structure Constraints, IEEE Conference on Computer Vision and Pattern Recognition (CVPR), pp. 2745–2753, 2016.

[2] A. Tanihata, M. Tanaka and M. Okutomi, Alignment and fusion of visible and infrared images based on gradient-domain processing, Proceedings of IS&T Electronic Imaging (EI2022), Vol.34, Issue.10, pp.366-1 – 366-5, 2022

[3] G. Chen, F. Zhu and P.A. Heng, An efficient statistical method for image noise level estimation, Proceedings of the IEEE International Conference on Computer Vision, pp. 477-485, 2015.

[4] A. Mittal, A. K. Moorthy and A. C. Bovik, No-reference image quality assessment in the spatial domain, IEEE Transactions on image processing. Vol.21, Issue.12, pp. 4695–4708, 2012.

[5] P. Pérez, M. Gangnet and A Blake, Poisson image editing, ACM SIGGRAPH Papers, pp. 313–318, 2003.

[6] R. Krutsch and D. Tenorio, Histogram equalization. Freescale Semiconductor, Document Number AN4318, Application Note, 2011.

[7] K. Zuiderveld, Contrast Limited Adaptive Histogram Equalization, Chapter VIII.5, Graphics Gems IV. P.S. Heckbert (Eds.), Cambridge, MA, Academic Press, pp. 474-485, 1994.

[8] S. M. Pizer, E. P. Amburn, J. D. Austin and R. Cromartie , Adaptive histogram equalization and its variations, Computer vision, graphics, and image processing, Vol.39, Issue.3, pp. 355-368, 1987.

[9] J. Ma, Y. Ma and C. Li, Infrared and visible image fusion methods and applications: A survey, Information Fusion, Vol.45, pg. 153-178, 2019.

[10] Y. Ogino, T. Shibata, M. Tanaka and M. Okutomi, Coaxial visible and FIR camera system with accurate geometric calibration, Proceedings of SPIE Defense + Commercial Sensing (DCS2017), Vol.10214, pp.1021415-1-6, 2017.

[11] T. Shibata, M. Tanaka and M. Okutomi, LWIR image visualization preserving local details and global distribution by gradient-domain image reconstruction, Proceedings of SPIE Defense + Commercial Sensing (DCS2017), Vol.10178, pp.101780X-1-11, 2017.

[12] T. Rukkanchanunt, M. Tanaka and M. Okutomi, Full thermal panorama from a long wavelength infrared and visible camera system, Journal of Electronic Imaging, Vol.28, Issue.3, pp.033028-1-10, 2019.

[13] F. Suard, A. Rakotomamonjy, A. Bensrhair and A. Broggi, Pedestrian detection using infrared images and histograms of oriented gradients, IEEE Intelligent Vehicles Symposium, 2006.

[14] M. Bertozzi, A. Broggi, T. Fascioli, G. Graf and M. Meinecke, Pedestrian detection for driver assistance using multiresolution infrared vision, IEEE Transactions on Vehicular Technology, Vol.53, pp. 1666–1678, 2004.

[15] C. Dai, Y. Zheng, and X. Li, Pedestrian detection and tracking in infrared imagery using shape and appearance, Computer Vision and Image Understanding, Vol. 106, pp. 288–299, 2007.

[16] L. Zhang, B. Wu, and R. Nevatia, Pedestrian detection in infrared images based on local shape features, IEEE Conference on Computer Vision and Pattern Recognition, pp. 1—8, 2007.

[17] B. Fardi, U. Schuenert and G. Wanielik, Shape and motion-based pedestrian detection in infrared images: A multi sensor approach, Proceeding of the IEEE Intelligent Vehicles Symposium, pp. 18–23, 2005.

[18] R. Usamentiaga, P. Venegas, J. Guerediaga, L. Vega, J. Molleda and F.G. Bulnes, Infrared thermography for temperature measurement and non-destructive testing, Sensors, Vol. 14, pp. 12305–12348, 2014.

[19] P. Venegas, E. Ivorra, M. Ortega and I. S. Ocáriz, Towards the Automation of Infrared Thermography Inspections for Industrial Maintenance Applications, Sensors, Vol. 22.2, 2022.

[20] K. Stokowiec, D. Kotrys-Działak, D. Mochocka and M. Sokołowski, Heat and power plant chimneys thermal inspection with an infrared camera, E3S Web of Conferences. Vol. 336, 2022.

[21] Y. Liao, X. Jiang, Z. Zhang, H. Zheng, T. Li and Y. Chen, The Influence of Wind Speed on the Thermal Imaging Clarity Based Inspection for Transmission Line Conductors, IEEE Transactions on Power Delivery, VOl. 38, pp. 2101–2109, 2022.

Author Biography

Taichi Nakano received his bachelor's degree from Tokyo Institute of Technology, Tokyo, Japan, in 2022. He is currently a master's student at Tokyo Institute of Technology.

Masayuki Tanaka received his Ph.D. degree from Tokyo Institute of Technology, Tokyo, Japan, in 2003 and joined Agilent Technology. He was a research scientist at Tokyo Institute of Technology from 2004 to 2008, a visiting scholar at Stanford University from 2013 to 2014. He is currently a professor at Tokyo Institute of Technology.

Masatoshi Okutomi received his master's degree from Tokyo Institute of Technology in 1983 and joined Canon Inc., Tokyo, Japan. He was a visiting research scientist at Carnegie Mellon University, PA, USA from 1987 to 1990. He received his Ph.D. degree from Tokyo Institute of Technology in 1993. He is currently a Professor at Tokyo Institute of Technology.